JOURNAL OF GEOPHYSICAL RESEARCH, VOL. 115, D14303, doi:10.1029/2009JD012731, 2010

An aircraft-based upper troposphere lower stratosphere O_3, CO, and H_2O climatology for the Northern Hemisphere

S. Tilmes,[1] L. L. Pan,[1] P. Hoor,[2] E. Atlas,[3] M. A. Avery,[4] T. Campos,[1] L. E. Christensen,[5] G. S. Diskin,[4] R.-S. Gao,[6] R. L. Herman,[5] E. J. Hintsa,[7,8] M. Loewenstein,[4] J. Lopez,[4] M. E. Paige,[9] J. V. Pittman,[1] J. R. Podolske,[4] M. R. Proffitt,[10] G. W. Sachse,[4] C. Schiller,[11] H. Schlager,[12] J. Smith,[7] N. Spelten,[11] C. Webster,[5] A. Weinheimer,[1] and M. A. Zondlo[13]

Received 26 June 2009; revised 24 February 2010; accepted 11 March 2010; published 22 July 2010.

[1] We present a climatology of O_3, CO, and H_2O for the upper troposphere and lower stratosphere (UTLS), based on a large collection of high-resolution research aircraft data taken between 1995 and 2008. To group aircraft observations with sparse horizontal coverage, the UTLS is divided into three regimes: the tropics, subtropics, and the polar region. These regimes are defined using a set of simple criteria based on tropopause height and multiple tropopause conditions. Tropopause-referenced tracer profiles and tracer-tracer correlations show distinct characteristics for each regime, which reflect the underlying transport processes. The UTLS climatology derived here shows many features of earlier climatologies. In addition, mixed air masses in the subtropics, identified by O_3-CO correlations, show two characteristic modes in the tracer-tracer space that are a result of mixed air masses in layers above and below the tropopause (TP). A thin layer of mixed air (1–2 km around the tropopause) is identified for all regions and seasons, where tracer gradients across the TP are largest. The most pronounced influence of mixing between the tropical transition layer and the subtropics was found in spring and summer in the region above 380 K potential temperature. The vertical extent of mixed air masses between UT and LS reaches up to 5 km above the TP. The tracer correlations and distributions in the UTLS derived here can serve as a reference for model and satellite data evaluation.

Citation: Tilmes, S., et al. (2010), An aircraft-based upper troposphere lower stratosphere O_3, CO, and H_2O climatology for the Northern Hemisphere, *J. Geophys. Res.*, *115*, D14303, doi:10.1029/2009JD012731.

1. Introduction

[2] The strong coupling between chemistry, dynamics and radiation in the upper troposphere/lower stratosphere (UTLS) makes this region very susceptible to climate variability and climate change [e.g., *Forster and Shine*, 1999; *Shepherd*, 2007]. The tropopause separates the stratosphere from the troposphere and marks the transition from the relatively unstable troposphere to the stratosphere, which is characterized by a high static stability. The tropopause acts as a barrier to exchange of air between the troposphere and the stratosphere due to the increasing thermal stratification in the vertical direction and increasing isentropic potential vorticity in the horizontal direction.

[3] The layer around the tropopause (TP) is therefore characterized by a strong gradient in chemical composition between stratospheric and tropospheric air masses. This layer is referred to as the extratropical transition layer (ExTL) [*World Meteorological Organization*, 2003; *Pan et al.*, 2004, 2007; *Hegglin et al.*, 2009] and it follows the local tropopause rather than isentropic surfaces [e.g., *Hoor et al.*, 2004; *Pan et al.*, 2004]. The depth of the ExTL has been quantified in earlier studies using O_3-CO and O_3-H_2O tracer correlations using aircraft [*Pan et al.*, 2004, 2007] and satellite observations [*Hegglin et al.*, 2009]. *Pan et al.* [2007] calculated the depth of the transition layer to be 1.5–2 km using O_3-H_2O correlations for the spring to fall season based on POLARIS aircraft observations. They found that the transition layer was centered at the thermal tropo-

[1]Atmospheric Chemistry Division, National Center of Atmospheric Research, Boulder, Colorado, USA.
[2]Institute for Atmospheric Physics, University Mainz, Mainz, Germany.
[3]Department of Marine and Atmospheric Chemistry, RSMAS, University of Miami, Miami, Florida, USA.
[4]NASA Ames Research Center, Moffett Field, California, USA.
[5]Jet Propulsion Laboratory, Pasadena, California, USA.
[6]Earth System Research Laboratory, NOAA, Boulder, Colorado, USA.
[7]Department of Chemistry and Chemical Biology, Harvard University, Cambridge, Massachusetts, USA.
[8]Global Monitoring Division, NOAA, Boulder, Colorado, USA.
[9]Southwest Sciences, Inc., Santa Fe, New Mexico, USA.
[10]Proffitt Instruments, Austin, Texas, USA.
[11]ICG-1, Research Center Jülich, Jülich, Germany.
[12]Institute for Physics of the Atmosphere, Wessling, Germany.
[13]Center for Mid-Infrared Technologies for Health and the Environment, Department of Civil and Environmental Engineering, Princeton University, Princeton, New Jersey, USA.

0148-0227/10/2009JD012731

pause, which was identified using the temperature lapse rate [*World Meteorological Organization*, 1957]. *Hegglin et al.* [2009] found a wider ExTL of 3–4 km based on O_3-CO and 2.5–4 km based on O_3-H_2O correlations with the center slightly above the TP, using data from the Atmospheric Chemistry Experiment Fourier Transform Spectrometer (ACE-FTS) satellite instrument. They only found minor seasonal differences in the depth of the ExTL. Using tracer-tracer correlation as applied in earlier studies, the ExTL includes observations above the layer of the strongest gradient in chemical composition. The depth of this layer can vary depending on the criteria used to define the stratospheric background. Resulting differences in the thickness of the ExTL between aircraft and satellite observations might be partly caused by different criteria chosen, as we discuss later.

[4] In addition to mixing processes at the TP, various studies have observed quasi-horizontal two-way exchange between tropospheric and stratospheric air masses in the vicinity of the subtropical jet (STJ) and the polar jet (PJ). Transport from the tropical troposphere across the barrier of the STJ [e.g., *Haynes and Shuckburgh*, 2000; *Hegglin et al.*, 2005] contributes to the chemical composition of the lowermost stratosphere (LMS). This influence has been quantified to range between 30% in winter and 65–70% in summer [*Hoor et al.*, 2005; *Bönisch et al.*, 2009]. In addition, the extratropics are influenced by air that has crossed the tropical tropopause and is transported up to 450 K potential temperature and subsequently to higher latitudes, where it descends and affects the composition of the LMS [e.g., *Rosenlof et al.*, 1997; *Tuck et al.*, 1997]. Furthermore, tropospheric intrusions associated with breaking Rossby waves influence the trace gas composition in the LMS [*Pan et al.*, 2009]. In addition, the influence of stratospheric mixing has been identified in the tropical troposphere, such as the large fraction of stratospheric ozone in the tropical upper troposphere, identified by *Marcy et al.* [2004] using HCl/O_3 tracer correlations.

[5] An accurate representation of the interplay between the complex processes in the UTLS in global chemistry climate models and chemistry transport models is of great importance in simulating present and future climate [e.g., *Law et al.*, 2000; *Hegglin et al.*, 2006; *Strahan et al.*, 2007; *Pan et al.*, 2007; *Teyssèdre et al.*, 2007]. Models are especially challenged to simulate the strong tracer gradient across the tropopause and the seasonality of mixing processes between UT and LS. A comprehensive UTLS climatology that describes the characteristics of tracer profiles across the TP is useful for model evaluation. This work is especially motivated by the on-going effort of process-oriented chemistry-climate model validation (CCMVal) [*Eyring et al.*, 2005, 2007], which includes the chemical composition of UTLS as well as the chemical transition across the TP. This climatology is also useful for satellite evaluation.

[6] High-resolution trace gas data from research aircraft over the last several decades provide a wealth of information for process studies in the UTLS region. These data have the strength of high accuracy and characterization of realistic atmospheric variability, such as the strong gradients across the tropopause [e.g., *Tuck et al.*, 2003; *Pan et al.*, 2004; *Poberaj et al.*, 2007], and the gradients across the STJ and PJ [e.g., *Ray et al.*, 2004; J. Lelieveld et al., personal communication, 1997]. UTLS tracer climatologies based on different aircraft databases have been established in earlier studies mainly in the stratosphere [e.g., *Tuck et al.*, 1997; *Boering et al.*, 1995; *Strahan et al.*, 1999]. For the lowermost stratosphere there are studies of the ExTL based on measurements taken in Europe over two years from the SPURT campaign [*Hoor et al.*, 2004; *Krebsbach et al.*, 2006; *Bönisch et al.*, 2009]. Furthermore, data from commercial airliners within MOZAIC [*Thouret et al.*, 2006; *Brioude et al.*, 2008], CARIBIC [*Zahn and Brenninkmeijer*, 2003] and the Global Atmospheric Sampling Program (GASP) [*Poberaj et al.*, 2007, 2009] provide a large amount of data in the tropopause region along the major flight routes. However, these data rarely reach 13 km and stay below the 360 K potential temperature level, and therefore do not cover the entire LMS or the tropical UTLS. Furthermore, the compiled data sets are limited in meridional and latitudinal coverage and the polar regions are not well characterized. For the tropics, a separate UTLS climatology was derived by *Folkins et al.* [2006] using data from the SHADOZ ozonesonde network and Aura Microwave Limb Sounder (MLS).

[7] The objective of this paper is two-fold. First, we present a novel approach to group sparse aircraft observations into three meteorological regimes: the tropics, the subtropics, and the polar region. Information about the height of the TP at each measurement location is used, which is correlated to the location of the jet streams. The separation of air masses following the large amplitude wave motions results in distinct tracer characteristics in each region. We propose simple criteria based on the tropopause height that can be applied to a large number of observations, as well as to model output, allowing model comparisons with non-co-located measurements.

[8] The second objective of this paper is to present a climatology of ozone (O_3), water vapor (H_2O), and carbon monoxide (CO) in the northern hemisphere UTLS. We apply the new method to high-resolution trace gas data from research aircraft experiments between 1995 and 2008. The interannual variability in this period is expected to be small for the considered tracers. The resulting climatology greatly improves the horizontal and vertical coverage of previous studies where aircraft data were used [*Pan et al.*, 2004, 2007]. Tracer distributions described here are referenced to the height of the thermal tropopause. The derived distributions provide a good representation of the strong gradient across the TP and can serve as a basis for comparison to model and satellite observations. The new climatology provides further insights into the seasonal and regional variability of tracer profiles and mixing processes in the UTLS. We use tracer-tracer correlations in the subtropics and the polar region to derive the depth of the region that is influenced by both stratospheric and tropospheric air masses, called the "mixing region" in the following. Here, we separate the mixing region in different vertical layers to characterize air mass exchange and mixing in altitudes referenced to the TP and to the vertical location of the STJ for different regions and seasons.

2. Data and Meteorological Analysis

2.1. Aircraft Observations

[9] We use data from a large collection of research aircraft campaigns as listed in Table 1. Measurements from projects

Table 1. All Aircraft Campaigns Included in This Study, Conducted Between May 1995 and June 2008

Campaign	Full Name	Period
STRAT	STratospheric TRacers of Atmospheric Transport	May 1995; Oct.–Nov. 1995; Feb., July Sep., Dec. 1996
TOTE/VOTE	Tropical Ozone Transport Experiment (TOTE) Vortex Ozone Transport Experiment (VOTE)	Dec. 1995–Feb. 1996
POLARIS	Photochemistry of Ozone Loss in the Arctic Region in Summer	April–May, June–July, Sep. 1997
SOLVE	SAGE III Ozone Loss and Validation Experiment	Nov. 1998; Sep.–Dec. 1999; Jan.–March 2000
SPURT	Spurenstofftransport in der Tropopausenregion	Nov. 2001 to July 2003, 8–10 flights per season [*Engel et al.*, 2006]
CRYSTAL-FACE	Cirrus Regional Study of Tropical Anvils and Cirrus Layers Florida Area Cirrus Experiment	July 2002
AVE	Aura Validation Experiment	
AVE Fall		October, November 2004
AVE Houston		June 2005
Polar AVE		January, February 2005
CR-AVE	Costa Rica	January, February 2006
TC4	Tropical Composition, Cloud and Climate Coupling	June–August 2007
START08/ preHIPPO	Stratosphere-Troposphere Analyses of Regional Transport HIAPER Pole-to-Pole observations (HIPPO)	April–June 2008
ARCTAS	Arctic Research of the Composition of the Troposphere from Aircraft and Satellites	April and June 2008
GRACE	POLARCAT - Greenland Aerosol and Chemistry Experiment	July 2008

not included in this analysis, e.g., MOZAIC, can be included in future studies using the procedures discussed here. The spatial and seasonal coverage of the flights included in the climatology is illustrated in Figures 1 and 2. The compiled data cover altitudes up to 22 km for measurements from the NASA ER-2 and WB57 aircraft, up to 15 km for measurements from the NSF/NCAR Gulfstream V (GV), formerly referred to as HIAPER (High-performance Instrumented Airborne Platform for Environmental Research), up to 13 km for the German Learjet, and up to 12 km for the NASA DC8, and the German Falcon. The collection of data obtained aboard these different aircraft results in a broad altitude coverage and sampling across the TP in nearly all latitudes in winter and summer. In fall, the

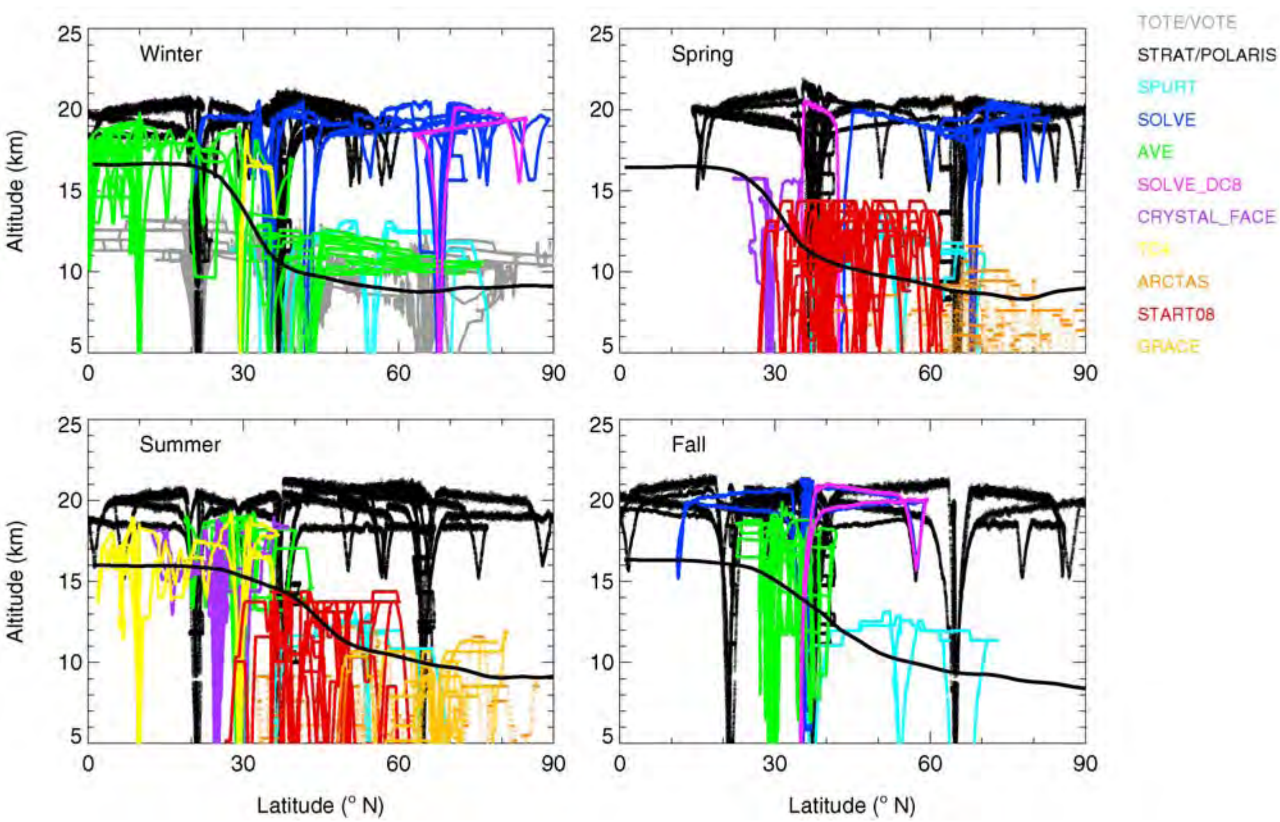

Figure 1. Vertical and latitudinal coverage of aircraft campaigns used here are grouped into four seasons: winter (DJF), spring (MAM), summer (JJA), and fall (SON). An averaged thermal tropopause for each seasons was derived for each season based on NCEP/FNL meteorological analysis of the year 2006, shown as a black line.

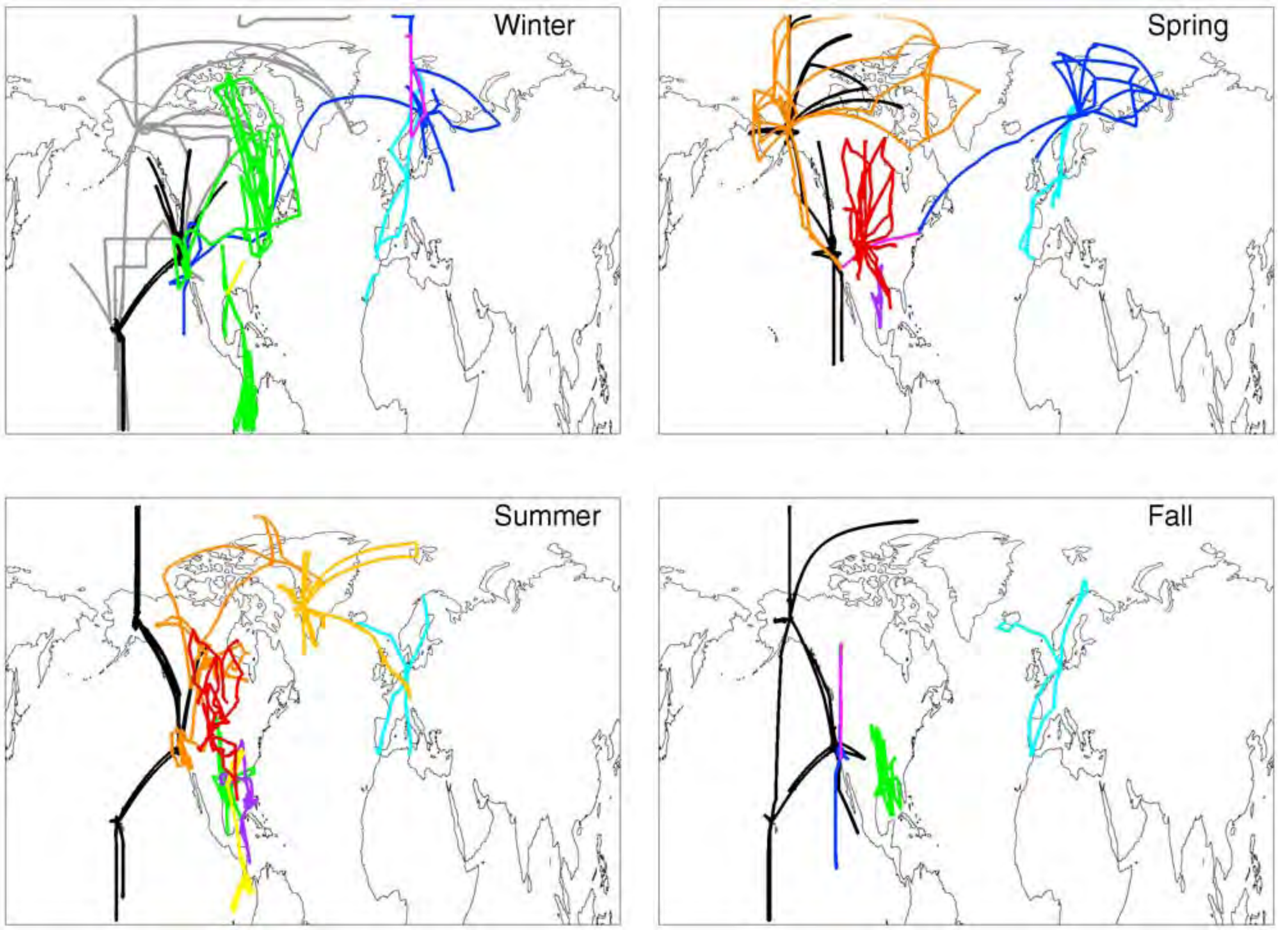

Figure 2. Horizontal and latitudinal coverage of different aircraft campaigns (colors as in Figure 1).

coverage of the middle and high latitudes is relatively sparse compared to the other seasons. All tracer data analyzed here are available during all seasons and latitude regimes, except for CO in the tropics during the spring time. In the horizontal, the observations cover a large part of North America and Western and Northern Europe for all seasons. No aircraft observations over Asia or Africa are included.

[10] The research aircraft and the payload vary for the different campaigns. The different instruments that were used to measure O_3, CO, and H_2O, are briefly summarized in Table 2. Here, we combine data with different integration times between 1 second and up to 30–40 seconds.

2.2. Meteorological Analysis

[11] NCEP Global Tropospheric Analyses (http://wwwt.emc.ncep.noaa.gov/gmb/para/parabout.html) are used to derive the location of the STJ and PJ, based on calculation of the zonal wind maximum. We also derive the local thermal TP, both primary and secondary, using the temperature lapse rate [*World Meteorological Organization*, 1957]. Further, we derive the local TP for every measurement (see Section 4). Before September 1999, we use analyses from the Final Global Data Assimilation System (FNL) on a global grid of 2.5 × 2.5 degree every 12 hours. The analyses are available on the surface and at 16 levels from 1000 hPa to 10 hPa. To calculate the TP height for aircraft data taken after September 1999, we use FNL analyses on a 1.0 × 1.0 degree global grid, which are available on 26 levels from 1000 hPa to 10 hPa and every 6 hours. Due to the coarse vertical resolution, we quadratically interpolate meteorological data to a finer pressure grid to estimate the cold point and therefore the TP height as precisely as possible. The relatively coarse vertical resolution of meteorological analyses in the vicinity of the TP of ≈1 km before 1999 contributes to increased uncertainties in our estimate of the TP height, and therefore to increased uncertainties in tracer profiles referenced to the TP height. Differences between TP height derived using meteorological data and TP height derived using temperature profiles during the flight are often in the range of ±1 km. However, differences in the range of ±2 km were found for some campaigns. Since these deviations occur in both directions, an impact on the following analysis is expected to mainly affect the variability and not the mean value of the tracer distribution with regard to the TP.

3. Definition of Meteorological Regimes in the UTLS

[12] The UTLS can be broadly divided into the tropical UTLS and the extratropical UTLS (ExUTLS), separated by the discontinuity of the thermal tropopause that occurs at the

Table 2. Summary of Instrumentation, Accuracy, and Precision of Ozone, CO, and H_2O for Different Aircraft Campaigns for Various Years Between 1995 and 2008 and on Different Carriers

Campaign	Carrier	Year	Ozone Instrument	Precision/ Accuracy	CO Instrument	Precision/ Accuracy	H_2O Instrument	Precision/ Accuracy
STRAT	ER2	1995/1996	UVP[a]	±5%/±5%	ALIAS[b]	<0.2 ppbv/3%	Harvard H_2O[c]	±5%/0.1 ppmv
TOTE/VOTE	DC8	1995/1996	Cl[d]	0.9–1.9 ppbv/5%	DACOM[e]	<1%/<2%	DLH[f]	2%/10%
POLARIS	ER2	1997	UVP[a]	±5%/±5%	ALIAS[b]	<0.2 ppbv/3%	Harvard H_2O[c]	±5%/0.1 ppmv
SOLVE	ER2	1999	UVP[a]	±5%/±5%	ALIAS[b]	<0.2 ppbv/3%	Harvard H2O[c]	±5%/0.1 ppmv
SOLVE	DC8	1999	FastOz[g]	<1 ppbv/<2%	DACOM[e]	<1%/<2%	DLH[f]	2%/10%
SPURT	Learjet 35	2001–03	JOE (UVP)[a]	<3%/<5%	TRISTAR[h]	<1%/<2%	not used[i]	
CRYSTAL-FACE	WB57	2002	UVP[a]	±5%/±5%	Argus[j]	<2%	Harvard H2O[c]	±5%/0.25 ppmv
AVE Fall	WB57	2004	UVP[a]	±5%/±5%	not used[i]		JPL H2O[k]	<1%/10%
AVE Houston	WB57	2005	UVP[a]	±5%/±5%	Argus[j]	<2%	JPL H2O[k]	<1%/10%
PAVE	DC8	2005	FastOZ[g]	2%/<1%	DACOM[e]	<1%/<2%	DLH[f]	2%/10%
CR-AVE	WB57	2006	UVP[a]	±5%/±5%	ALIAS[b]	<0.2 ppbv/3%	Harvard H2O[c]	±5%/0.25 ppmv
TC4	WB57	2007	UVP[a]	±5%/±5%	WAS[l]	5%/10%	JPL H2O[k]	<1%/10%
START08	GV	2008	UVP[a]	±5%/±5%	NCAR CO[m]	0.8 ppbv/±9%	VCSEL[n]	<3%/10%
ARCTAS	DC8	2008	Cl[d]	0.9–1.9 ppbv/5%	DACOM[e]	<1%/<2%	DLH[f]	2%/10%
GRACE	Falcon	2008	UVP[a]	2%/5%	VUV[o]	5%/10%	FISH[p]	4%/0.2 ppmv

[a]Dual-beam UV-absorption ozone photometer [*Proffitt and McLaughlin*, 1983; *Krebsbach et al.*, 2006] for the JOE (Jülich Ozone Experiment during SPURT) and modified for GRACE using the TE49C instrument [*Schlager et al.*, 1997].
[b]Aircraft laser infrared absorption spectrometer [*Webster et al.*, 1994; *Lopez et al.*, 2008].
[c]Photofraqment Fluorescence Hygrometer, Harvard [*Weinstock et al.*, 1994; *Hintsa et al.*, 1998, 1999].
[d]Chemiluminescence Instrument [*Ridley and Robinson*, 1992]. Precision values were derived for 1-second values and vary with altitude.
[e]Diode Laser In-Situ (DACOM) [*Sachse et al.*, 1987].
[f]Diode Laser Hygrometer (DLH) [*Vay et al.*, 2000; *Diskin et al.*, 2002; *Podolske et al.*, 2003].
[g]FastOz Chemiluminescence Instrument.
[h]Tracer in-situ TDLAS (tunable diode laser absorption spectrometer) for atmospheric research [*Hoor et al.*, 2004].
[i]Measurements are not included, because some profiles systematic discrepancies in comparison to averaged values, derived combining other campaigns for the same season, that could not be explained.
[j]Argus tunable diode laser spectrometer [*Loewenstein et al.*, 2002].
[k]Open-Path, Near-Infrared Tunable Diode Laser Spectrometer (JPL) [*May*, 1998].
[l]Whole Air Sampler CO.
[m]NCAR/NSF C-130 CO vacuum UV resonance fluorescence instrument, similar to that of *Gerbig et al.* [1999]. Precision and accuracy were derived for a 1-minute averaging time and estimated based on the good agreement with the Harvard instrument.
[n]VCSEL hygrometer (M. A. Zondlo et al., Vertical cavity laser hygrometer for the National Science Foundation Gulfstream-V aircraft, submitted to Journal of Geophysical Research, 2010).
[o]VUV fluorescence (AL5002) [*Baehr et al.*, 2003].
[p]Ly alpha photo fragment fluorescence (FISH) [*Zöger et al.*, 1999].

location of the STJ. Previous studies have shown that there is also a strong quasi-horizontal gradient in the ozone field across the STJ and the PJ [e.g., *Hudson et al.*, 2003; *Ray et al.*, 2004; *Brioude et al.*, 2008] and in water vapor [*Follette-Cook*, 2008]. These observations and the results of our analyses, to be discussed later, motivate a further subdivision of the ExUTLS into the subtropics and the polar regions. Following *Hudson et al.* [2003], we divide the UTLS in three regions, the tropics, subtropics and the polar region, that are separated by two daily varying boundaries the STJ and the PJ.

[13] We introduce an approach to define coherent regimes that are based on tropopause height. This approach takes advantage of the well known relationship between the tropopause height change and the location of the STJ and the PJ [e.g., *Palmén and Newton*, 1969; *Shapiro and Gronas*, 1999]. Further, *Hudson et al.* [2003] have shown that the meteorological regimes defined by the locations of the jet streams describe characteristic TP heights. The air mass location relative to the jet streams can be therefore calculated using either wind fields or temperature fields.

[14] To define the characteristic height of the TP for each region, we analyze the seasonal varying distributions of the two correlated fields, as given in Figures 3 and 4 for two seasons. The TP height is given in potential temperature coordinate, which follows the isentropic movement of air masses and therefore serves as a better quantity than altitude coordinates. The STJ and PJ shown in Figure 3 and 4 were calculated using the local maximum of the zonal wind speed between 5–20 km along each longitude. Using the wind field to identify the location of the STJ and the PJ is rather complicated, as discussed in detail by *Koch et al.* [2006]. The simple criteria used here possibly leads to misidentifications of the STJ core and the PJ core, as shown below.

[15] The location of both the STJ and PJ varies strongly during each season and covers a large latitudinal area of about 30 degrees; see Figure 3. The tropics (equatorward of the STJ) cover the largest region in summer, whereas the polar region (poleward of the PJ) is extended towards lower latitudes in winter compared to summer. In addition, the STJ and the PJ are merged more often in summer compared to winter.

[16] Figure 4 shows the distribution of tropopause height (given in potential temperature) in the tropics, subtropics and polar regimes as identified by the zonal wind maxima. In general, the separation of tropics and subtropics is very distinct with a tropopause height change from ≈380 K to ≈340 K potential temperature. The separation between subtropics and polar region is less distinct, especially in summer. The overlap in tropopause height is consistent with the behavior of polar jet, which is often segmented and

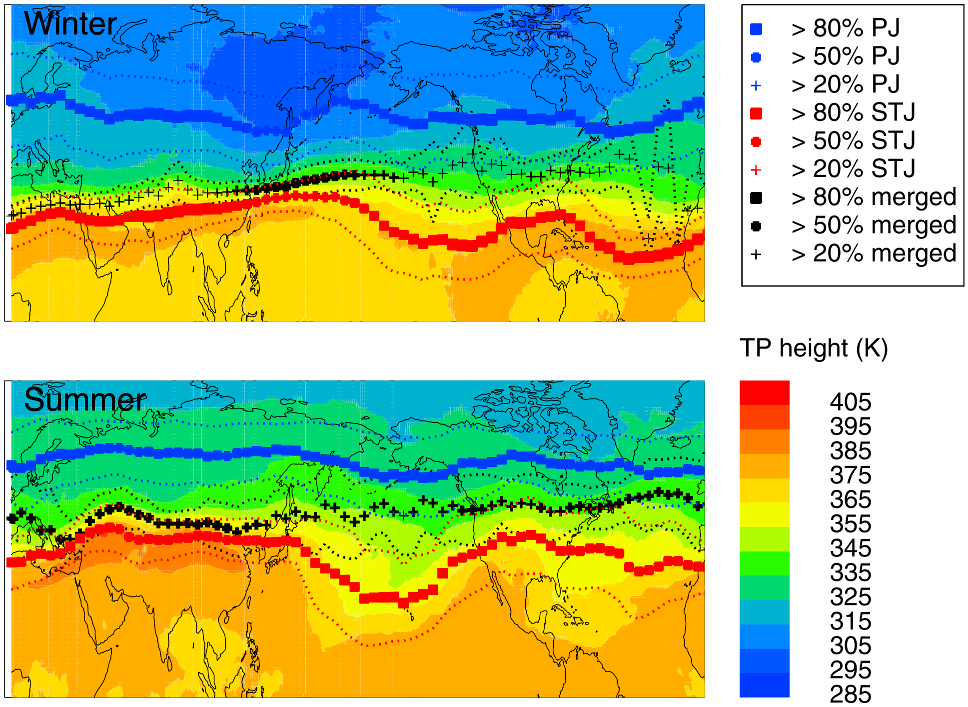

Figure 3. Horizontal map of averaged primary thermal TP height for (top) winter and (bottom) summer. In addition, the location of the maximum zonal wind velocity (minimum of 20 m/s) of the STJ (red) and the PJ (blue) are shown. Cases where STJ and PJ are merged are shown in back. Thickness of the symbols indicate the frequency of occurrence of the STJ and PJ, or a merged jet, during each season, based on NCEP/FNL meteorological analysis in 2006. Meteorological analysis, available four times a day, are grouped in different seasons. If more than two wind maximum were calculated, the location of the furthermost jet stream is used.

meridionally oriented and forms a less continuous boundary. In winter, there is a minor population of high tropopauses (380 K or higher) found in the subtropics. In summer, there is a small group of low tropopauses (below 360 K) found to be equatorward of the STJ. These examples show the uncertainties that arise in using the wind field to define the location of the STJ core and the PJ core, which result in a frequent misalignment of the jet streams and the location of the break of the TP (Figure 4).

[17] Nevertheless, a statistically valid correlation can be derived based on Figures 3 and 4. A high TP at ≈370–380 K potential temperature (≈17 km) is characteristic of the tropics. In the subtropics, the TP height decreases from ≈370–380 K potential temperature (17 km) in the tropics to below 325 K potential temperature (8–10 km) in the polar region. The polar region, poleward of the PJ, is characterized by a low TP height around 310–325 K potential temperature (8–10 km) depending on season. We define criteria that are empirically chosen, to achieve the most distinct tracer characteristic in each of the three regimes. These criteria are partly based on the relationship between TP height and the jet locations, including the seasonal variation of the TP height poleward of the PJ. We also include information on multiple TP events in these criteria. In the presence of a double TP near the STJ, the primary TP is often tilted towards potential temperature levels below 325 K. Those regions are included in the subtropics to prevent air masses with subtropical characteristics from being incorrectly added to the polar region.

[18] We summarize the regions and criteria below.

[19] 1. The "tropics" are defined as a regime where TP heights are larger than 365 K potential temperature for all seasons. Besides the upwelling of air masses from the troposphere into the stratosphere, exchange with stratospheric air from higher latitudes influences the characteristics of these air masses [e.g., *Rosenlof et al.*, 1997; *Tuck et al.*, 1997].

[20] 2. The "subtropics" are defined as a regime where the height of the TP is between 325 and 365 K (winter and spring) and between 335 and 365 K (summer and fall). In addition to considering the height of the primary TP, locations with multiple TP events are also included in this regime.

[21] 3. The "polar region" is defined as a regime where the TP is located at or below 325 K in winter and spring and at or below 335 K in summer and fall, or poleward of 65°N. The TP height is located below 325 K (335 K) for most of the profiles poleward of the PJ (see Figure 4). In high latitudes, the WMO-derived TP can occur above 335 K or cannot be identified, even though almost all profiles are located poleward of the PJ. Therefore, all measurements taken poleward of 65°N are assigned to the polar region, independent of the TP height.

[22] Using new criteria based on the TP height instead of using the wind field is done to simplify and clarify the

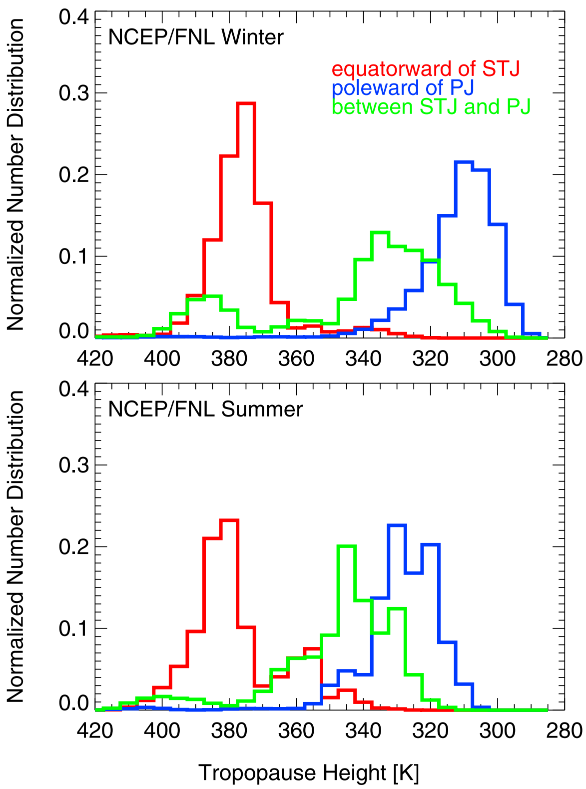

Figure 4. Normalized number distribution of the tropopause potential temperature (K) of the primary TP, for three dynamical regimes defined using the location of the subtropical jet (STJ) and the polar jet (PJ) for (top) winter and (bottom) summer. The location of the jet stream is defined as the location of the maximum zonal wind velocity (minimum of 20 m/s) in the Northern Hemisphere between 10 and 85°N. The STJ is defined as the wind maximum furthest equatorward of the jet stream, the PJ is defined as the furthest poleward jet stream detected. The first distribution covers all data points equatorward of the STJ (red), the second, all data points between the STJ and the PJ (if STJ and PJ are not merged) (green), and the third covers all data points poleward of any zonal wind maximum (blue).

definition of the three meteorological regimes so they can be applied consistently to different sets of observations and model results. In this way the influence of mixing above and below the core of the jet stream and the TP in each region can be investigated if considering tropopause-referenced altitude coordinates.

4. UTLS Climatology of O_3, CO, and H_2O

[23] The criteria introduced in the last section are applied to the collection of aircraft observations. In this section we present the resulting climatology of O_3, CO, and H_2O tracer profiles referenced to the TP and O_3-tracer correlations. We describe specific features that can be identified using this climatology. Further, we quantify the depth of the mixing region between UT and LS in the ExUTLS for different altitude levels and for different seasons.

[24] The climatology is compiled as trace gas profiles in tropopause referenced coordinates, defined as the modified altitude. For each observation made at a geometric altitude Z, its modified altitude Z_m, is calculated as:

$$z_m = z_{mTP} + (Z - Z_{TP}), \qquad (1)$$

where Z_{TP} is the co-located tropopause height, Z_{mTP} is the mean tropopause height for all observations in one region and season. The co-located tropopause height for each measurement is derived using meteorological analyses as discussed in Section 2.2. Adjusting the relative altitude by the mean tropopause height of each region and season highlights seasonal and regional differences in the tracer distribution and of the mean TP height. In addition, observations can be evaluated relative to the TP height, which allows one to separate the variability of trace gases due to transport and chemistry from the variability of the TP height (as discussed by *Pan et al.* [2004] and *Birner* [2006]).

[25] For statistical analysis, the distributions of profiles in modified altitude is presented using probability distribution functions (PDFs) (see Figure 5, middle). PDFs are determined for one km altitude bins. We compare different regions and seasons using the median and the quartiles (25% and 75%) of the tracer distributions (Figure 5). We discuss next the characteristics of the example shown in Figure 5.

4.1. O_3, CO, and H_2O Profiles Relative to the TP

[26] The separation of aircraft data into the meteorological regimes defined here distinguishes significant differences in the tracer behavior. PDFs of modified altitude profiles of O_3, CO, and H_2O for tropics, subtropics, and the polar region are shown for summer in Figure 6. The distributions in the tropics and the polar region are in general more compact compared to the subtropics.

[27] In the tropics, ozone increases from low tropospheric values of ≈100 ppbv at around 12 km towards higher values up to 400 ppbv at the TP. On the other hand, CO and H_2O mixing ratios start decreasing at around 10 km (≈6 km below the TP) from their tropospheric value (70–120 ppbv for CO and values larger than 100 ppmv for H_2O) towards the smaller values of ≈40–60 ppbv for CO and 6–7 ppmv for H_2O at the TP. Above the TP, O_3 mixing ratios increase rapidly (see Figure 6, left).

[28] In the subtropics, O_3 mixing ratios start decreasing slightly below the TP. Above the TP the distribution of O_3 profiles shows a bimodal distribution between 0–4 km above the TP. Correspondingly, the median of the distribution shows a weaker slope in this region. The rather low ozone mixing ratios below 200 ppbv up to 4 km above the TP indicate isentropic influence of tropical air masses, as further discussed below. In agreement, CO mixing ratios start decreasing at the TP until they reach stratospheric values at ≈6 km above the TP. High CO mixing ratios of up to 120 ppbv are still found up to 2–3 km above the TP in summer. The tropospheric CO distribution is much wider in the subtropics than in the tropics and shows 20% larger CO mixing ratios. In contrast, H_2O mixing ratios start decreasing at ≈5 km below the TP until they reach their minimum at 3 km above the TP in summer. Similar to CO, relatively large H_2O mixing ratios of up to 10–15 ppmv exist at up to 2 km above the TP in summer.

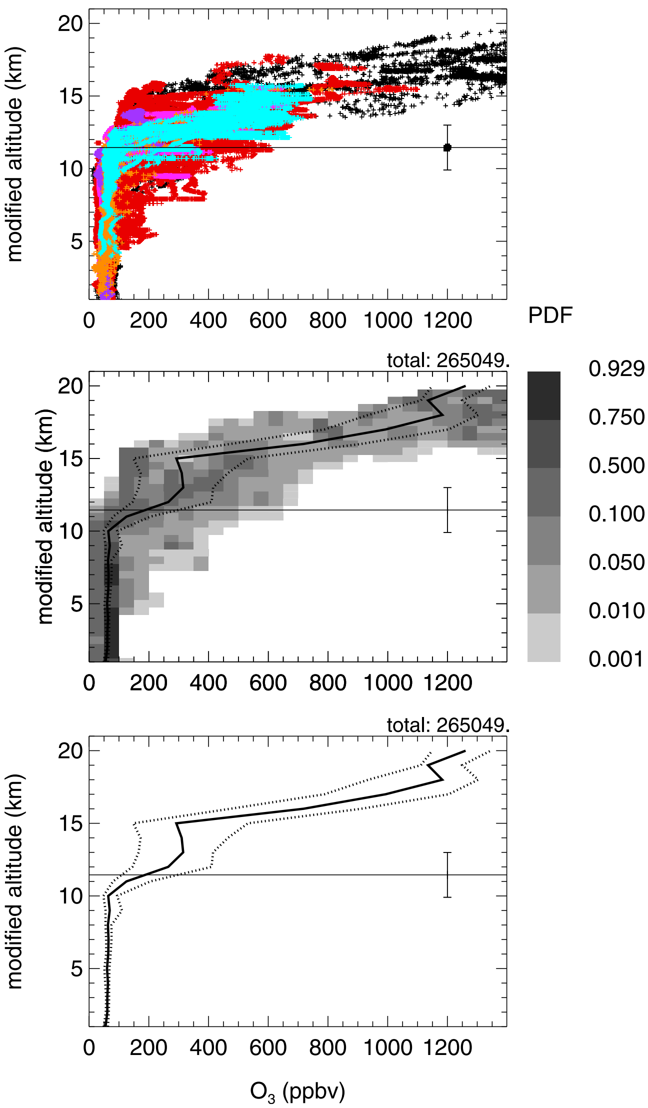

Figure 5. Ozone profiles versus modified altitude for aircraft campaigns in spring in the subtropics. The average of TP heights for each measurement point is shown as a black horizontal line; the standard deviation is shown as an error bar. (top) All selected aircraft observations are shown, different colors indicate different campaigns (see Figure 1.) (middle) Probability distribution function of all aircraft observations shown in the top panel. Total number of data points is given on the top right of the middle and bottom plots. The median of the distribution is shown as black solid line and the quartiles of the distribution (25% and 75%) as black dotted lines. (bottom) Same as Figure 5 (middle) but without the probability distribution function.

[29] In the polar region, vertical profiles of all three tracers are relatively compact. In contrast to the subtropics, a strong gradient across the TP appears in the polar region. The the change in slope of tracer profiles up to 5 km above the TP is characteristic of the tracer behavior of the LMS, as has been observed in earlier studies [e.g., *Hoor et al.*, 2004, 2005]. Enhanced H_2O and CO mixing ratios in 2–3 km above the TP indicate the influence of convection above the TP in summer [e.g., *Fischer et al.*, 2002]. Maximum CO mixing ratios around 5 km below the TP are likely a result of long-range transport and convection of high levels of CO from polluted regions in the subtropics.

[30] Seasonal variation of the distinct characteristics of tracer PDFs in each of the defined regions are less pronounced and in general much smaller than regional variations and are also smaller than the variability of each region (see Figure 6). The median profiles of the tracer PDFs for each season and region are illustrated in (Figure 7). The largest variability between different seasons occurs in the subtropics. In this region, the mean tropopause height varies strongly between the seasons with the lowest TP in winter and spring and the highest TP in summer and fall. In addition, this region is characterized by a decreasing TP between the tropics and the polar region, which results in a standard deviation of the TP height of 2–4 km. The largest variability of the height of the TP was found in fall. The median tracer profile based on a partly bimodal distribution especially in the subtropics varies depending on the importance of each of the modes and therefore on the characteristics of single aircraft campaigns. Seasonal differences of median profiles based on sparse aircraft data are therefore not very significant and have to investigated in further studies using additional observations. Nevertheless, the seasonal cycle of ozone in the tropical UT can be identified with lowest ozone mixing ratios occurring in winter [*Folkins et al.*, 2006]. Further, the sensitivity of H_2O to temperature at and above the TP can be identified, know as the "tape recorder" effect [*Mote et al.*, 1996; *Krebsbach et al.*, 2006]. H_2O mixing ratios show smallest values in winter and spring and largest in summer and fall at 1–2 km above the TP for both tropics and subtropics and at the TP in the polar region.

[31] The climatology compiled here is in general in agreement with findings from earlier studies. Similar feature are found, as described by *Folkins et al.* [2006] for the tropics, and as shown by *Logan* [1999] using ozone sonde observations. The tracer distributions are further in agreement with earlier aircraft observations in the UT and up to 12–13 km in the LS for the subtropics and polar region [e.g., *Novelli et al.*, 2003; *Thouret et al.*, 2006; *Brioude et al.*, 2008; *Krebsbach et al.*, 2006; *Poberaj et al.*, 2009] and with satellite observations [*Hegglin et al.*, 2009]. The strongest tracer gradient within 2 km around the TP was found in the polar region. This result differs from that calculated using satellite observations, which is likely due to a much finer vertical resolution of aircraft data compared to satellite observations. The climatology extends the results of earlier studies by revealing significant differences in the shape of tropopause referenced tracer profiles in the three regions of tracers.

4.2. Tracer-Tracer Correlations Using O_3, CO, and H_2O in the ExUTLS

[32] We further investigate the influence of mixing processes between tropospheric and stratospheric air masses in different vertical layers of the UTLS with regard to the TP and the STJ core. O_3-tracer correlations have been used to identify irreversible mixing between the UT and LS in the ExUTLS [e.g., *Hintsa et al.*, 1998; *Ray et al.*, 1999; *Fischer et al.*, 2000; *Zahn et al.*, 2000; *Hoor et al.*, 2002, 2004; *Pan*

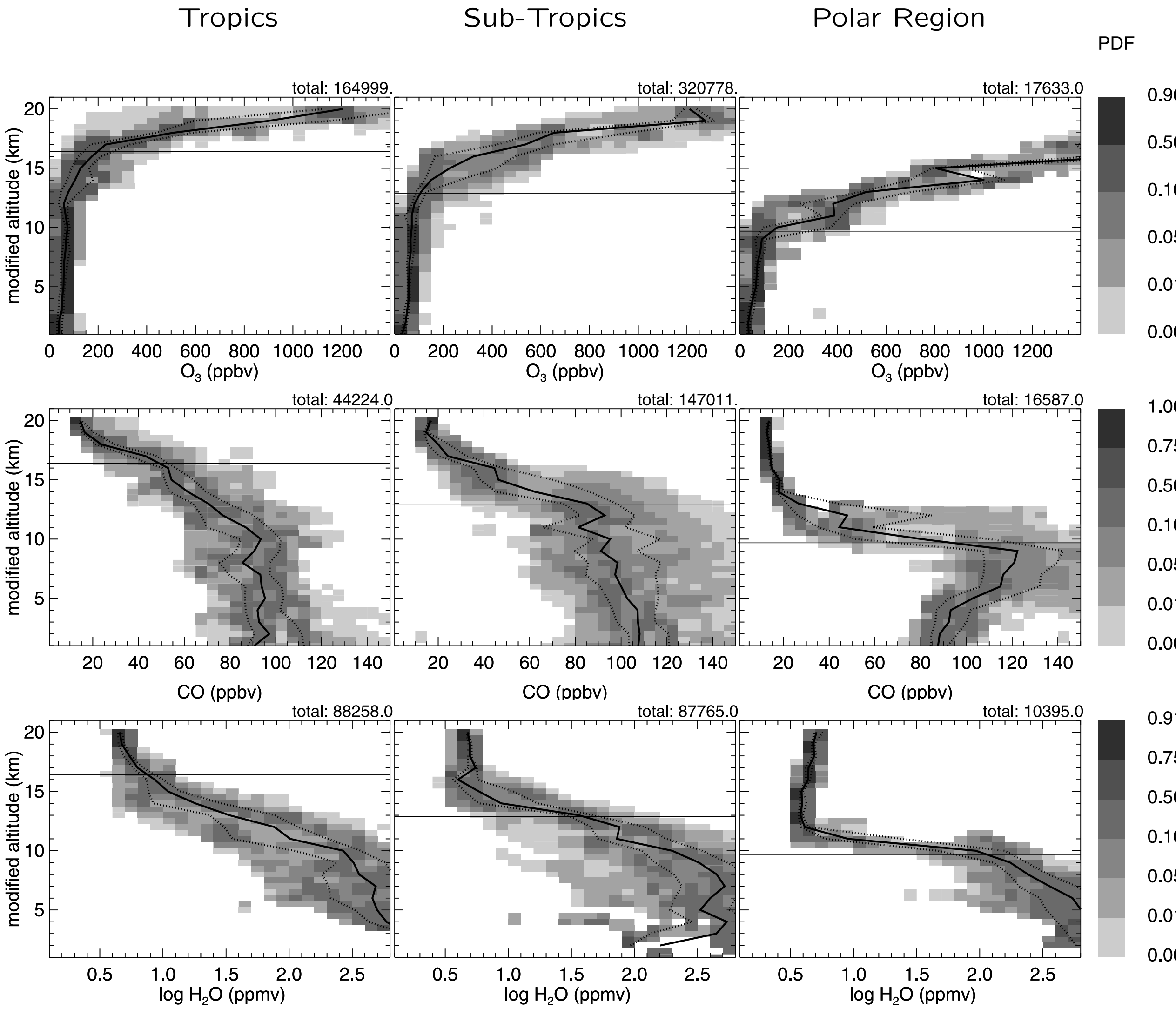

Figure 6. Same as Figure 5 (middle) but for (top) O_3, (middle) CO, and (bottom) H_2O and for different meteorological regions in summer. H_2O is plotted on a logarithmic scale.

et al., 2004, 2007]. The distribution of tracer-tracer correlation between a stratospheric tracer and a tropospheric tracer can be separated into a stratospheric branch, a tropospheric branch, and a region of mixed air masses. In the case of no mixing, one would expect an "L"-shape tracer-tracer correlation [e.g., *Fischer et al.*, 2000; *Hoor et al.*, 2002; *Pan et al.*, 2004]. The shape of the distribution is therefore influenced by mixing processes between the end members of the mixing line, which are the background mixing ratios of the stratospheric tracer (here O_3) and the tropospheric tracer (CO and H_2O).

[33] The distribution of O_3-tracer correlations in subtropics and the polar region are significantly different (Figure 8). For the subtropics, the mixing region is wider than in the polar region for both O_3-CO and O_3-H_2O correlations. The increased spread of the correlation is caused by a greater variability in the tropospheric entry mixing ratios of different tracers. In addition, a bimodal distribution appears in the subtropics between the 100 and 400 ppbv ozone level. One mode shows lower CO mixing ratios (40–60 ppbv) and the other mode shows higher CO mixing ratios (50–100 ppbv) (see Figure 8, top left). In the O_3-H_2O correlation, one branch of the bimodal distribution is characterized by very low stratospheric H_2O mixing ratios. The low ozone values accompanied by low CO and H_2O mixing ratios suggest that air in the LMS has mixed with dehydrated air and air with lower CO that has a source region in the TTL. Therefore, we define the mode with low CO mixing ratios to be the "higher altitude mode" and the other to be the "lower altitude mode", as further discussed below. In the polar region, the shape of tracer correlations is more compact and only the branch with higher CO mixing ratios exists in this example.

[34] To quantify the influence of mixing in different horizontal regions of the ExUTLS, we have chosen a stratospheric threshold of 20 ppbv CO. This is the stratospheric background of CO of 12–15 ppbv [*Flocke et al.*, 1999; *Herman et al.*, 1999] plus 5 ppbv to include the uncertainty of the observations used (Figure 8, red lines). Different from earlier studies [*Pan et al.*, 2004, 2007; *Hegglin et al.*, 2009], the stratospheric branch is not defined by O_3-CO values in the LMS. Instead, we use stratospheric

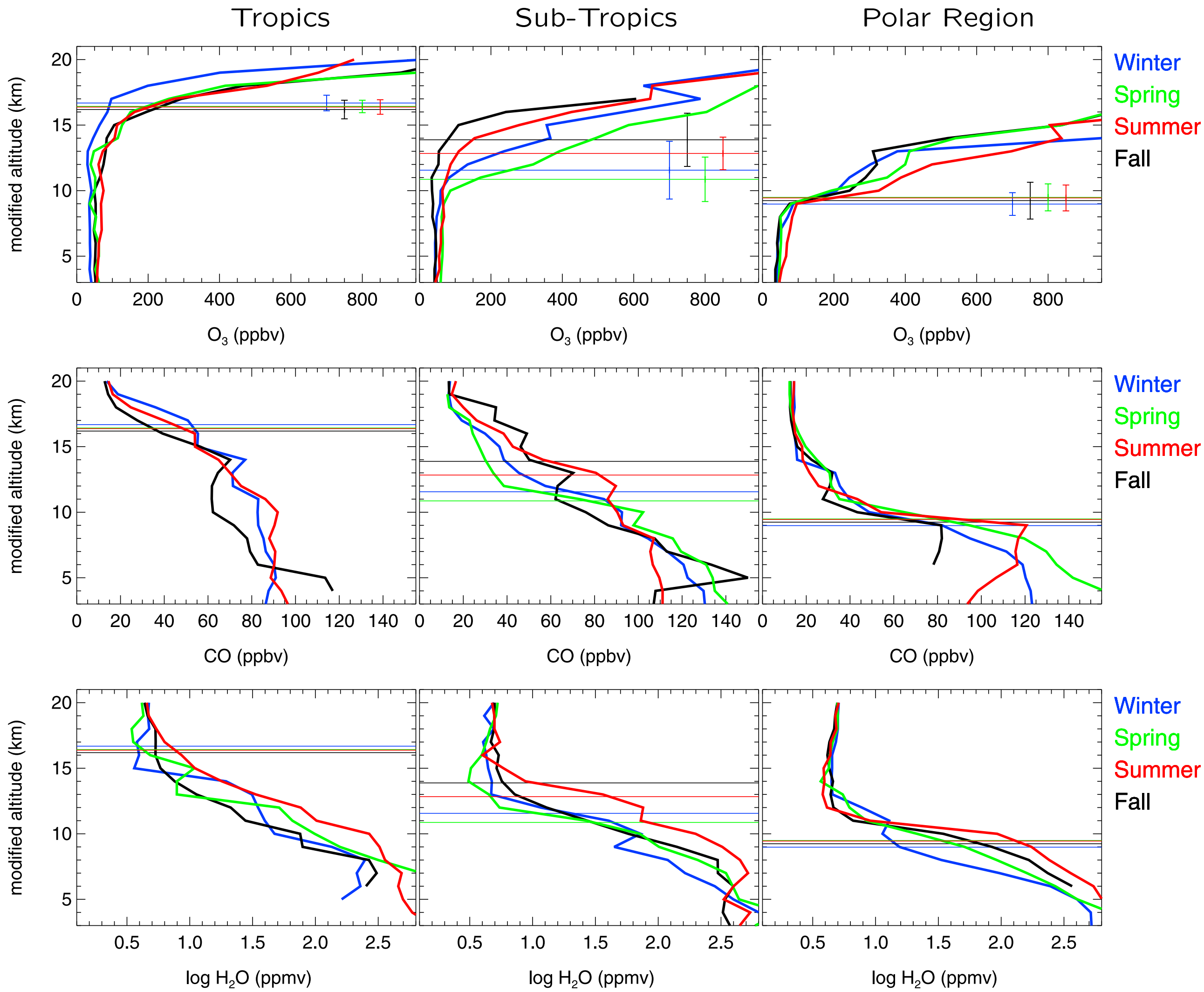

Figure 7. Averaged modified altitude profiles of (top) O_3, (middle) CO, and (bottom) H_2O, for the three defined regions. Different colors of profiles show different seasons. The averaged TP derived from all observations in each seasons is shown as a colored line with a standard deviation shown as colored horizontal error bars. H_2O is plotted on a logarithmic scale.

background CO values. The mixing region as define here includes mixed air masses in the ExTL as well as in the LMS. To separate mixed air masses in ExTL and LMS we use information from the vertical tracer profiles.

[35] For O_3-H_2O correlations, a H_2O value of ≈7 ppmv would be adequate to use as the stratospheric threshold for all seasons and regions. However, in the case of H_2O as the tropospheric tracer, the influence of dehydrated air masses with a source in the TTL can result in deviations of the O_3-H_2O correlation from the "L"-shape towards lower H_2O mixing ratios. Those data cannot be distinguished from unmixed air masses using a stratospheric threshold value of 7 ppmv and the depth of the mixing region cannot be identified. Therefore, we will not consider O_3-H_2O correlations in the following to derive the depth of the mixing region. The tropospheric threshold is set to 80 ppbv of O_3 in fall to spring and 100 ppbv in summer, to address the changing background O_3 in the troposphere (Figure 8, green lines). Note, tropospheric pollution can result in higher O_3 values than the chosen threshold, and therefore induces an uncertainty in the derived region of mixed air masses.

[36] To investigate the location of mixed air masses in the tracer-tracer space for different altitude regions, we divide all data into four vertical layers based on theta levels, as shown in Figure 9, which is an example for spring in the subtropics. The first layer is defined to include all observations that are located in the mixing region above the 380 K potential temperature level (Figure 9b, left). This region can be understood to be located above the STJ. Observations from this region describe the higher altitude mode of the bimodal distribution, as described above, and can be therefore identified as being influenced by air masses coming from the TTL. The second vertical layer, commonly defined as the LMS, includes observations in the mixing region that are located above the ExTL (as defined next) and below the 380 K potential temperature level (Figure 9b, right). For the subtropics, this region is influenced by quasi horizontal exchange or small scale processes associated with the strong wind shear at the STJ. For the polar region, this

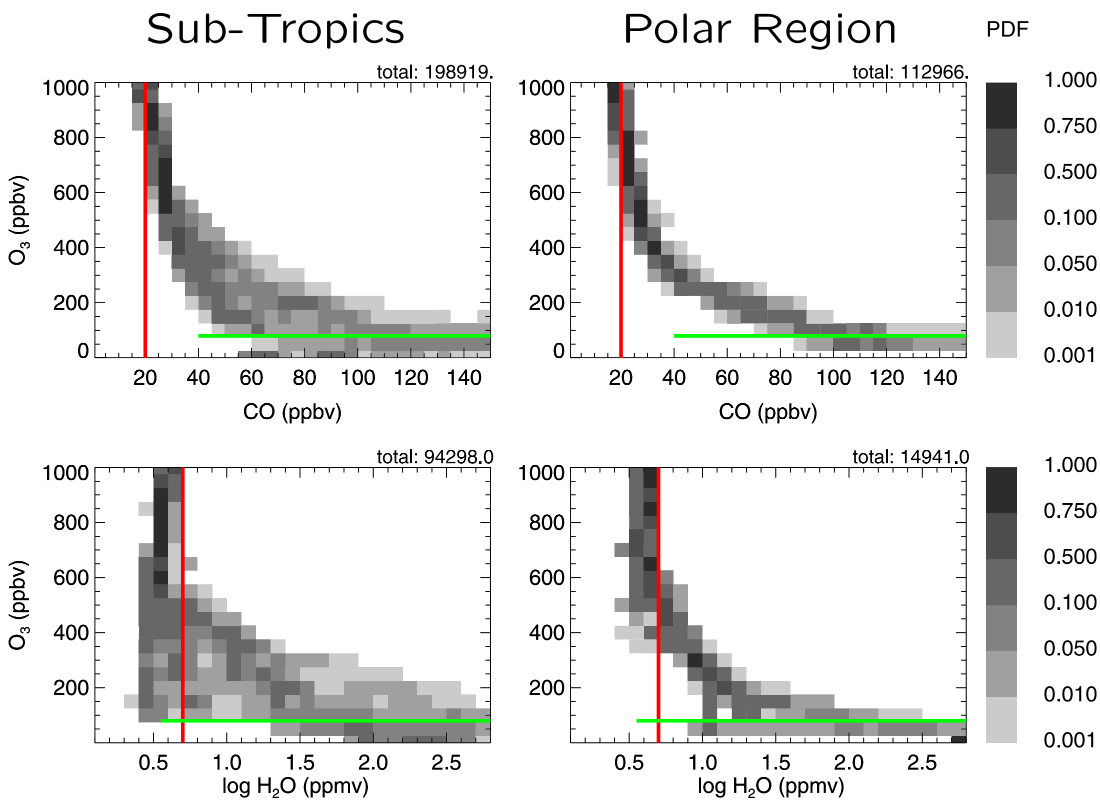

Figure 8. Probability distribution functions of (top) O_3-CO correlations and (bottom) O_3-H_2O correlations derived from all aircraft observations for (left) subtropics and (right) the polar region in spring. Total number of data is given on the top right of each plot. The threshold for the stratospheric background values is shown in red and for the tropospheric background value in green (see text for more details). H_2O is plotted on a logarithmic scale.

layer shows evidence of the influence of quasi horizontal exchange processes from the STJ. The third vertical layer, denoted as the ExTL, is located close to the extra-tropical TP and includes all data within 10 K potential temperature below the TP and 15 K potential temperature above the TP. In this region the tracer gradient across the TP is strongest and air masses have had some degree of mixing across the TP (Figure 9c, left). The fourth vertical layer is defined to include all data below the ExTL. Mixed air masses in this layer can be attributed to stratospheric intrusion events that reach deep into the troposphere. Data points in, as well as below, the ExTL contribute for the most part to the lower altitude mode of the O_3-CO correlation.

[37] As shown above, mixed air masses that are located in different vertical layers above the TP significantly overlap in the tracer-tracer space. The two modes shown in the tracer-tracer space can be approximately assigned to air masses above the ExTL in around 2–5 km (higher altitude mode) and in and below the ExTL (lower altitude mode). However, a vertical separation of mixed air masses, for example between ExTL and the LMS, is not straight forward based on tracer-tracer correlations alone. The mixing region identified by the tracer correlations critically depends on the criteria chosen to define the tropospheric and stratospheric background.

[38] Here, we identify the location of mixed air masses between UT and LS in the tracer-tracer space including information about the altitude distance of the observations from the TP. The depth of the mixing region for the different vertical layers is summarized in Figure 10 for all seasons in the subtropics and polar region. For this analysis we derive a histogram of the distribution of the mixing region using 1 km bins. The histogram is normalized with all measurements available for each specific altitude bin to eliminate the uneven sampling of data for the different altitudes.

[39] For spring and summer, the contribution of mixed air masses above 380 K potential temperature is very pronounced and well separated from mixed air masses in the ExTP (Figure 9, green lines). 70–90% of all sampled data in the altitude range of 2–6 km above the TP can be identified as mixed air masses with a source region in the upper tropical troposphere region. The strong influence of tropical-like air masses in the subtropics in spring, identified by the high altitude branch in the tracer-tracer correlations is likely a result of frequent tropospheric intrusions that occur around the 380 K potential temperature level [*Pan et al.*, 2009]. The large amount of mixed air masses in summer in these altitudes might be also connected to the Asian or North American monsoon anticyclone, which might result in enhanced isentropic transport of tropospheric air masses toward the subtropics above 380 K potential temperature. The presence of enhanced CO and H_2O mixing ratios in the subtropic above 380 K potential temperature are consistent with this transport pathway (not shown).

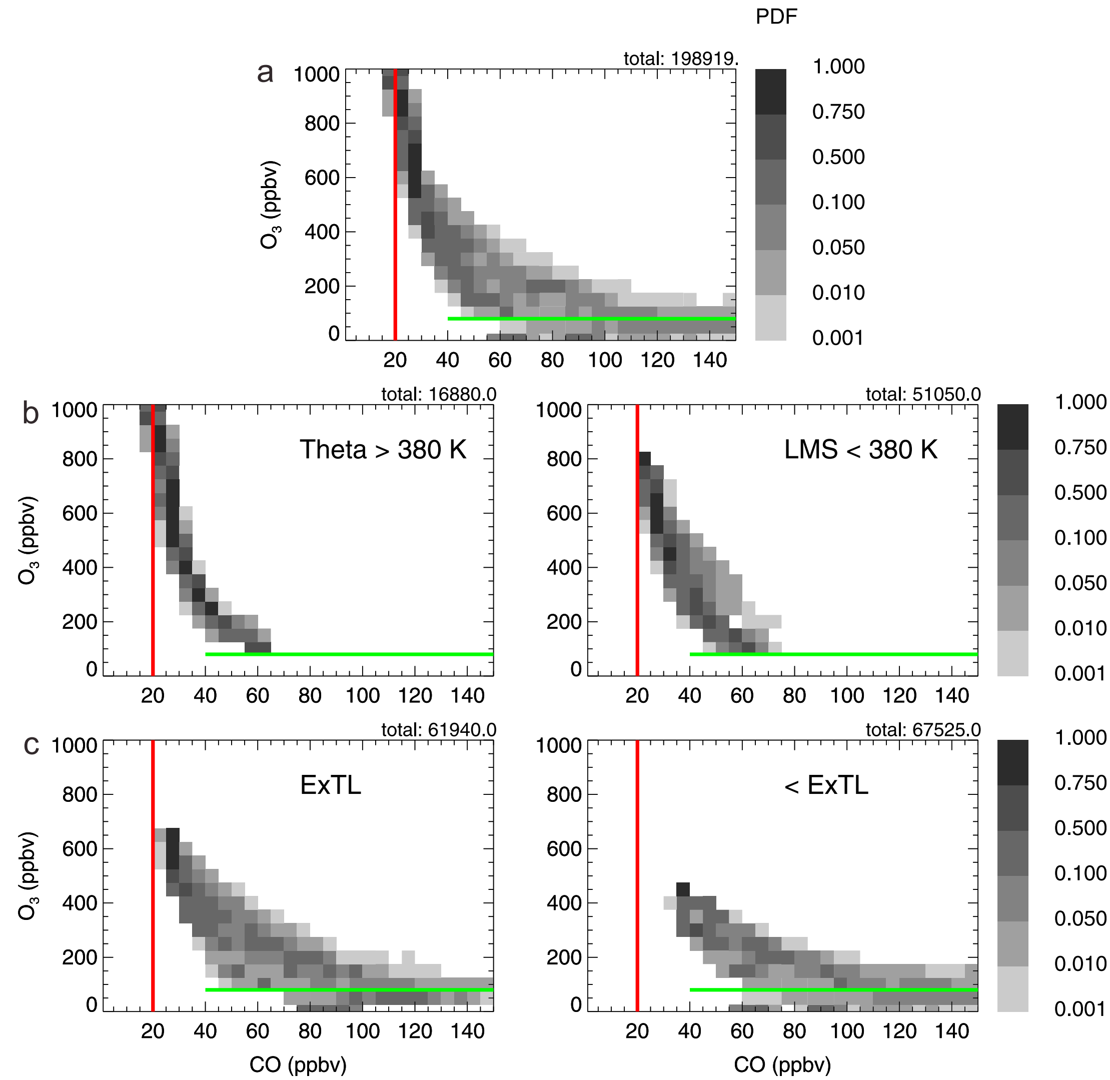

Figure 9. (a) Same as Figure 8 (top left). (b) Same as Figure 9a but only for data that were sampled (left) above the 380 K potential temperature level and (right) below the 380 K potential temperature level and above the ExTL. (c) (left) Same as Figure 9a but only for data that were sampled in a region above 15 K and below 10 K potential temperature around the TP, defined as ExTL. (right) Same as Figure 9a but only for data that were sampled below the ExTL.

[40] The contribution of mixed air masses between the ExTL and the 380 K potential temperature level (cyan lines) is largest in fall and winter in the subtropics. In summer and fall, the bimodal distribution of O_3-CO correlations in the subtropics disappears (not shown) and mixed air masses in different layers form a more compact distribution. The more frequent occurrence of double TP events [*Randel et al.*, 2007] in winter compared to summer seems to result in strong mixing events below the 380 K level and above the STJ in winter, during a time when the barrier at the STJ is strongest [*Haynes and Shuckburgh*, 2000]. Mixed air masses below the ExTL are most pronounced in spring and reach deeper than 5 km into the troposphere. For the polar region, the contribution of mixed air masses above 380 K is much smaller compared to the subtropics, as a result of the smaller influence of air masses that have a source region in the TTL. The strongest contribution of mixed air masses (and therefore the influence of tropospheric air masses in the LMS) occurs between the ExTL and the 380 K level (cyan lines), which is characteristic of the LMS. The depth of the mixing layer for the ExTL and the LMS derived here is different from earlier studies based on satellite observations [*Hegglin et al.*, 2009], because the aircraft data used in our analysis provide a higher spatial resolution across the TP, and we use different criteria to define the ExTL.

[41] The derived location and depth of the mixing region between the UT and LS are also influenced by uncertainties in the derived location of the TP height. A comparison between the derived TP heights using in-situ temperature profiles and those derived using meteorological analyses can show maximum differences up to ±2 km. Uncertainties in the position of the thermal TP of up to 1–2 km are likely, due to the coarse vertical resolution of meteorological analysis used, especially for the earlier campaigns that are analyzed here. However, the derived values serve as robust estimates given the large amount of data. The derived depth

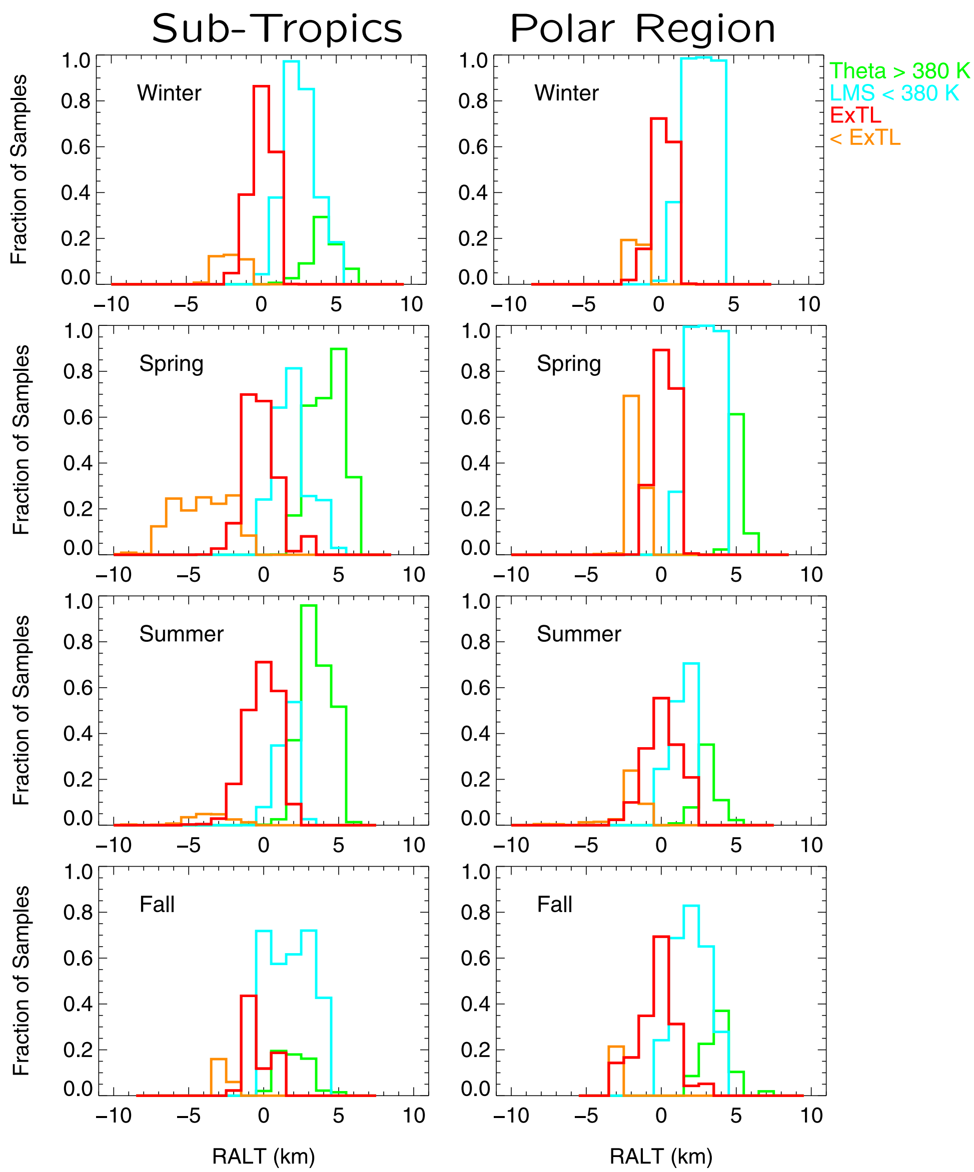

Figure 10. The histograms show the normalized distribution of the mixed samples of data that are located in the transition region between the upper troposphere and the lowermost stratosphere in different altitude levels relative to the thermal tropopause (see legend) using 1 km bins for different seasons and for the (left) subtropics and (right) polar region.

of the mixing regions described here should therefore be seen as an upper limit.

5. Summary and Conclusions

[42] A UTLS climatology has been compiled for O_3, CO, and H_2O using aircraft measurements taken between 1995 and 2008 over North America and Western and Northern Europe. The measurements from the campaigns analyzed here cover a broad latitudinal and vertical range in the UTLS for most of the seasons in the Northern Hemisphere. A novel set of criteria is introduced to group data into three regions: the tropics, subtropics, and the polar region, by using the height of the tropopause at each measurement location. The derived aircraft climatology shows distinct tracer characteristics in each of the three regions, which reflects the influence of differences in dynamics, source distributions and tropopause temperature (in the case of H_2O).

[43] For the tropics, only those measurements that are located in a region with a high tropopause (>365 K potential temperature, about 17 km) are included. Exchange across the subtropical tropopause at the location of the subtropical jet affects the TTL and results in enhanced ozone values up to 3 km below the TP. H_2O and CO do not show a strong gradient at the TP, but show a maximum decrease around 14–15 km in the TTL at the altitude of maximum convective outflow. The "tape recorder" effect in H_2O is well reproduced in this climatology.

[44] The subtropical part of the lowermost stratosphere is strongly influenced by bidirectional exchange in the vicinity of the STJ at the location of the subtropical tropopause break. This region is defined by the decreasing height of the

TP towards higher latitudes and the frequent occurrence of double TP events in connection with TST. The two-way exchange across the STJ and a large variability in the tropospheric tracer input level results in a bimodal distribution of tracer profiles and a bimodal mixing region in the tracer-tracer space, especially in spring and summer. The polar region is defined as a region with a low thermal tropopause north of the polar jet. Tracer profiles show a very strong gradient at the thermal tropopause in this region in ≈2 km around the TP. In addition, we identify a change in vertical gradient of tracer profiles that occur about 4–5 km above the TP in the LMS. The seasonal variation of the tracer distributions are in general much smaller than differences between the regions especially in the subtropics, due to a strongly varying TP height.

[45] In the tracer-tracer space the mixing region between stratospheric and tropospheric air masses is a composite of data that are observed in different vertical layers with regard to the TP. The depth of this region can be identified using tracer-tracer correlations. The extent of mixing in different vertical layers and the separation between ExTL and LMS is achieved using tropopause referenced tracer profiles. The region of mixing in a thin layer of ≈1–2 km above and below the TP describes the strongest tracer gradient in the ExUTLS. Enhanced influence of upper tropical tropospheric air masses at altitudes 2–6 km above the TP (above 380 K potential temperature) can be identified in spring and summer in the subtropics. In the polar region, the impact of mixing across the STJ and the PJ occurs at altitudes 1–5 km above the TP. The impact of deep stratospheric intrusions is most pronounced in spring at altitudes of 5–7 km below the TP.

[46] The data coverage of seasons, regions, and altitudes is not evenly distributed in the data set used for our analysis, and the different data coverage might impact our results. The number of observations in the polar region, especially in fall, is limited and further aircraft measurements are desirable that cover the entire UTLS. Overall, we have shown that an aircraft-based climatology is able to characterize the tracer behavior in different seasons and regions in the UTLS. The classification criteria introduced are simple and can be applied to a large amount of model results and satellite data. Therefore, this climatology is well suited for model and satellite evaluation studies, however it might be biased in using aircraft campaigns that targeted specific scientific questions. This climatology derived for O_3, CO and H_2O is planned to be extended to many different species measured during the campaigns used here and additional aircraft campaigns in future studies.

[47] **Acknowledgments.** This work is supported in part by the National Center for Atmospheric Research (NCAR) in support by the National Science Foundation and by the NASA Upper Atmosphere Program. Research at the Jet Propulsion Laboratory was performed under contract with NASA. Thanks are also due to NCEP Environmental Modeling Center (EMC) for providing meteorological analysis. The authors thank Louisa Emmons and Rolando Garcia for helpful comments and suggestions.

References

Baehr, J., H. Schlager, H. Ziereis, P. Stock, P. van Velthoven, R. Busen, J. Ström, and U. Schumann (2003), Aircraft observations of NO, NO_y, CO, and O_3 in the upper troposphere from 60°N to 60°S—Interhemispheric differences at midlatitudes, *Geophys. Res. Lett.*, *30*(11), 1598, doi:10.1029/2003GL016935.

Birner, T. (2006), Fine-scale structure of the extratropical tropopause region, *J. Geophys. Res.*, *111*, D04104, doi:10.1029/2005JD006301.

Boering, K. A., et al. (1995), Measurements of stratospheric carbon dioxide and water vapor at northern midlatitudes: Implications for troposphere-to-stratosphere transport, *Geophys. Res. Lett.*, *22*(20), 2737–2740.

Bönisch, H., A. Engel, J. Curtius, T. Birner, and P. Hoor (2009), Quantifying transport into the lowermost stratosphere using simultaneous in-situ measurements of SF6 and CO_2, *Atmos. Chem. Phys. Discuss.*, *8*, 21,229–21,264.

Brioude, J., J. P. Cammas, O. R. Cooper, and P. Nedelec (2008), Characterization of the composition, structure, and seasonal variation of the mixing layer above the extratropical tropopause as revealed by MOZAIC measurements, *J. Geophys. Res.*, *113*, D00B01, doi:10.1029/2007JD009184.

Diskin, G. S., J. R. Podolske, G. W. Sachse, and T. A. Slate (2002), Open-path airborne tunable diode laser hygrometer, *Proc. SPIE Int. Soc. Opt. Eng.*, *4817*, 196–204, doi:10.1117/12.453736.

Engel, A., et al. (2006), Observation of mesospheric air inside the Arctic stratospheric polar vortex in early 2003, *Atmos. Chem. Phys.*, *6*, 267–282.

Eyring, V., et al. (2005), A strategy for process-oriented validation of coupled chemistry-climate models, *Bull. Am. Meteorol. Soc.*, *86*(8), 1117–1133, doi:10.1175/BAMS-86-8-1117.

Eyring, V., et al. (2007), Multimodel projections of stratospheric ozone in the 21st century, *J. Geophys. Res.*, *112*, D16303, doi:10.1029/2006JD008332.

Fischer, H., F. G. Wienhold, P. Hoor, O. Bujok, C. Schiller, P. Siegmund, M. Ambaum, H. A. Scheeren, and J. Lelieveld (2000), Tracer correlations in the northern high latitude lowermost stratosphere: Influence of cross-tropopause mass exchange, *Geophys. Res. Lett.*, *27*(1), 97–100, doi:10.1029/1999GL010879.

Fischer, H., et al. (2002), Synoptic tracer gradients in the upper troposphere over central Canada during the Stratosphere-Troposphere Experiments by Aircraft Measurements 1998 summer campaign, *J. Geophys. Res.*, *107*(D8), 4064, doi:10.1029/2000JD000312.

Flocke, F., et al. (1999), An examination of chemistry and transport processes in the tropical lower stratosphere using observations of long-lived and short-lived compounds obtained during STRAT and POLARIS, *J. Geophys. Res.*, *104*, 26,625–26,642.

Folkins, I., P. Bernath, C. Boone, G. Lesins, N. Livesey, A. M. Thompson, K. Walter, and J. C. Witte (2006), Seasonal cycles of O_3, CO, and convective outflow at the tropical tropopause, *Geophys. Res. Lett.*, *33*, L16802, doi:10.1029/2006GL026602.

Follette, M. B., R. D. Hudson, and G. E. Nedoluh (2008), Classification of Northern Hemisphere stratospheric ozone and water vapor profiles by meteorological regime, *Atmos. Chem. Phys. Discuss.*, *8*, 13,375–13,411.

Forster, P., and K. P. Shine (1999), Stratospheric water vapour change as possible contributor to observed stratospheric cooling, *Geophys. Res. Lett.*, *26*(21), 3309–3312, doi:10.1029/1999GL010487.

Gerbig, C., S. Schmitgen, D. Kley, A. Volz-Thomas, K. Dewey, and D. Haaks (1999), An improved fast-response vacuum-UV resonance fluorescence CO instrument, *J. Geophys. Res.*, *104*, 1699–1704, doi:10.1029/1998JD100031.

Haynes, P., and E. Shuckburgh (2000), Effective diffusivity as a diagnostic of atmospheric transport: 2. Troposphere and lower stratosphere, *J. Geophys. Res.*, *105*, 22,795–22,810, doi:10.1029/2000JD900092.

Hegglin, M. I., D. Brunner, T. Peter, J. Straehelin, V. Wirth, P. Hoor, and H. Fischer (2005), Determination of eddy diffusivity in the lowermost stratosphere, *Geophys. Res. Lett.*, *32*, L13812, doi:10.1029/2005GL022495.

Hegglin, M. I., et al. (2006), Measurements of NO, NO_y, N_2O and O_3 during SPURT: Implications for transport and chemistry in the lowermost stratosphere, *Atmos. Chem. Phys.*, *6*, 1331–1350.

Hegglin, M. I., C. D. Boone, G. L. Manney, and K. A. Walker (2009), A global view of the extratropical tropopause transition layer ExTL from Atmospheric Chemistry Experiment Fourier Transform Spectrometer O_3, H_2O, and CO, *J. Geophys. Res.*, *114*, D00B11, doi:10.1029/2008JD009984.

Herman, R. L., et al. (1999), Measurements of CO in the upper troposphere and lower stratosphere, *Chem. Global Change Sci.*, *1*, 173–183.

Hintsa, E. J., et al. (1998), Troposphere-to-stratosphere transport in the lowermost stratosphere from measurements of H_2O, CO_2, N_2O and O_3, *Geophys. Res. Lett.*, *25*(14), 2655–2658, doi:10.1029/98GL01797.

Hintsa, E. J., E. M. Weinstock, J. G. Anderson, and R. D. M. May (1999), On the accuracy of in situ water vapor measurements in the troposphere and lower stratosphere with the Harvard Lyman-α hygrometer, *J. Geophys. Res.*, *104*, 8183–8198.

Hoor, P., H. Fischer, L. Lange, J. Lelieveld, and D. Brunner (2002), Seasonal variations of a mixing layer in the lowermost stratosphere as identified by the CO-O_3 correlation from in situ measurements, *J. Geophys. Res.*, *107*(D5), 4044, doi:10.1029/2000JD000289.

Hoor, P., C. Gurk, D. Brunner, M. I. Hegglin, H. Wernli, and H. Fischer (2004), Seasonality and extent of extratropical TST derived from in-situ CO measurements during SPURT, *Atmos. Chem. Phys.*, *4*, 1427–1442.

Hoor, P., H. Fischer, and J. Lelieveld (2005), Tropical and extratropical tropospheric air in the lowermost stratosphere over Europe: A CO-based budget, *Geophys. Res. Lett.*, *32*, L07802, doi:10.1029/2004GL022018.

Hudson, R. D., A. D. Frolov, M. F. Andrade, and M. B. Follette (2003), The total ozone field separated into meteorological regimes, part I: Defining the regimes, *J. Atmos. Sci.*, *60*, 1669–1677.

Koch, P., H. Wernli, and C. Davies (2006), An event-based jet-stream climatology and typology, *Int. J. Climatol.*, *26*, 283–301.

Krebsbach, M., C. Schiller, D. Brunner, G. Günther, M. I. Hegglin, D. Mottaghy, M. Riese, N. Spelten, and H. Wernli (2006), Seasonal cycles and variability of O_3 and H_2O in the UT/LMS during SPURT, *Atmos. Chem. Phys.*, *6*, 283–301.

Law, K., P.-H. Plantevin, V. Thouret, A. Marenco, W. A. H. Asman, M. Lawrence, P. J. Crutzen, J.-F. Muller, D. A. Hauglustaine, and M. Kanakidou (2000), Comparison between global chemistry transport model results and Measurement of Ozone and Water Vapor by Airbus In-Service Aircraft (MOZAIC) data, *J. Geophys. Res.*, *105*, 1503–1525.

Loewenstein, M., H. Jost, J. Grose, J. Eilers, D. Lynch, S. Jensen, and J. Marmie (2002), Argus: A new instrument for the measurement of the stratospheric dynamical tracers, N_2O and CH_4, *Spectrochim. Acta Part A*, *58*(11), 2329–2345.

Logan, J. A. (1999), An analysis of ozonesonde data for the troposphere: Recommendations for testing 3-D models and development of a gridded climatology for tropospheric ozone, *J. Geophys. Res.*, *104*, 16,115–16,150, doi:10.1029/1998JD100096.

Lopez, J. P., M. Luo, L. E. Christensen, M. Loewenstein, H. Jost, C. R. Webster, and G. Osterman (2008), TES carbon monoxide validation during two AVE campaigns using the Argus and ALIAS instruments on NASA's WB-57F, *J. Geophys. Res.*, *113*, D16S47, doi:10.1029/2007JD008811.

Marcy, T. P., et al. (2004), Quantifying stratospheric ozone in upper troposphere with in situ measurements of HCl, *Science*, *304*, 261–265, doi:10.1126/science.1093418.

May, R. D. (1998), Open-path, near-infrared tunable diode laser spectrometer for atmospheric measurements of H_2O, *J. Geophys. Res.*, *103*, 19,161–19,172.

Mote, P. W., et al. (1996), An atmospheric tape recorder: The imprint of tropical tropopause temperatures on stratospheric water vapor, *J. Geophys. Res.*, *101*, 3989–4006.

Novelli, P. C., K. A. Masarie, P. M. Lang, B. D. Hall, R. C. Myers, and J. W. Elkins (2003), Reanalysis of tropospheric CO trends: Effects of the 1997–1998 wildfires, *J. Geophys. Res.*, *108*(D15), 4464, doi:10.1029/2002JD003031.

Palmén, E., and C. W. Newton (1969), *Atmospheric Circulation Systems*, 114 pp., Academic, San Diego, Calif.

Pan, L. L., W. J. Randel, B. L. Gary, M. J. Mahoney, and E. J. Hintsa (2004), Definitions and sharpness of the extratropical tropopause: A trace gas perspective, *J. Geophys. Res.*, *109*, D23103, doi:10.1029/2004JD004982.

Pan, L. L., J. C. Wei, D. E. Kinnison, R. R. Garcia, D. J. Wuebbles, and G. P. Brasseur (2007), A set of diagnostics for evaluating chemistry-climate models in the extratropical tropopause region, *J. Geophys. Res.*, *112*, D09316, doi:10.1029/2006JD007792.

Pan, L. L., et al. (2009), Tropospheric intrusions associated with the secondary tropopause, *J. Geophys. Res.*, *114*, D10302, doi:10.1029/2008JD011374.

Poberaj, C. S., J. Staehelin, D. Brunner, V. Thouret, and V. Mohnen (2007), A UT/LS ozone climatology of the nineteen seventies deduced from the GASP aircraft measurement program, *Atmos. Chem. Phys.*, *7*, 5917–5936.

Poberaj, C. S., J. Staehelin, D. Brunner, V. Thouret, H. D. Backer, and R. Stübi (2009), Longterm changes in UT/LS ozone between the late 1970s and the 1990s deduced from the GASP and MOZAIC aircraft programs and from ozonesondes, *Atmos. Chem. Phys.*, *9*, 5343–5369.

Podolske, J. R., G. W. Sachse, and G. S. Diskin (2003), Calibration and data retrieval algorithms for the NASA Langley/Ames Diode Laser Hygrometer for the NASA transport and chemical evolution over the pacific (TRACE-P) mission, *J. Geophys. Res.*, *108*(D20), 8792, doi:10.1029/2002JD003156.

Proffitt, M. H., and R. J. McLaughlin (1983), Fast-response dual-beam UV absorption ozone photometer suitable for use on stratospheric balloons, *Rev. Sci. Instrum.*, *54*, 1719–1728.

Randel, W. J., D. J. Seidel, and L. L. Pan (2007), Observational characteristics of double tropopauses, *J. Geophys. Res.*, *112*, D07309, doi:10.1029/2006JD007904.

Ray, E. A., F. L. Moore, J. W. Elkins, G. S. Dutton, D. W. Fahey, H. Vömel, S. J. Oltmans, and K. H. Rosenlof (1999), Transport into the Northern Hemisphere lowermost stratosphere revealed by in situ tracer measurements, *J. Geophys. Res.*, *104*, 26,565–26,580.

Ray, E. A., K. H. Rosenlof, E. Richard, D. Parrish, and R. Jakoubek (2004), Distribution of ozone in the region of the subtropical jet: An analysis of in situ aircraft measurements, *J. Geophys. Res.*, *109*, D08106, doi:10.1029/2003JD004143.

Ridley, B. A., and E. Robinson (1992), Observatory photochemistry experiment, *J. Geophys. Res.*, *97*, 10,285–10,290.

Rosenlof, K. H., A. F. Tuck, K. K. Kelly, J. M. Russell, and M. P. McCormick (1997), Hemispheric asymmetries in the water vapor and inferences about transport in the lower stratosphere, *J. Geophys. Res.*, *102*, 13,213–13,234.

Sachse, G., G. Hill, L. Wade, and M. Perry (1987), Fast-response, high-precision carbon monoxide sensor using a tunable diode laser absorption technique, *J. Geophys. Res.*, *92*, 2071–2081.

Schlager, H., P. Konopka, P. Schulte, U. Schumann, H. Ziereis, F. Arnold, M. Klemm, D. Hagen, P. Whitefield, and J. Ovarlez (1997), In situ observations of aircraft emissions signatures in the north atlantic flight corridor, *J. Geophys. Res.*, *102*, 10,739–10,750.

Shapiro, M. A., and S. Gronas (Eds.) (1999), *The Life Cycles of Extratropical Cyclones*, Am. Meteorol. Soc., Bosten, Mass.

Shepherd, T. G. (2007), Transport in the middle atmosphere, *J. Meteorol. Soc. Jpn.*, *103*(85B), 165–191.

Strahan, S. E., M. Loewenstein, and J. Podolske (1999), Climatology and small-scale structure of lower stratospheric N_2O based on in situ observations, *J. Geophys. Res.*, *104*, 2195–2208.

Strahan, S. E., B. N. Duncan, and P. Hoor (2007), Observationally derived transport diagnostics for the lowermost stratosphere and their application to GMI chemistry and transport model, *Atmos. Chem. Phys.*, *7*, 1449–1477.

Teyssèdre, H., et al. (2007), A new tropospheric and stratospheric Chemistry and Transport Model MOCAGE-Climat for multi-year studies: Evaluation ofthe present-day climatology and sensitivity to surface processes, *Atmos. Chem. Phys.*, *7*, 5815–5860.

Thouret, V., J.-P. Cammas, B. Sauvage, G. Athier, R. Zbinden, P. Nédélec, P. Simon, and F. Karcher (2006), Tropopause referenced ozone climatology and inter-annual variability (1994–2003) from the MOZAIC programme, *Atmos. Chem. Phys.*, *6*, 1033–1051.

Tuck, A. F., et al. (1997), The Brewer-Dobson circulation in the light of high altitude in situ aircraft observation, *Q. J. R. Meteorol. Soc.*, *123*, 1–69.

Tuck, A. F., S. J. Hovde, R. S. Gao, and E. C. Richard (2003), Law of mass action in the Arctic lower stratospheric polar vortex January–March 2000: ClO scaling and the calculation of ozone loss rates in a turbulent fractal medium, *J. Geophys. Res.*, *108*(D15), 4451, doi:10.1029/2002JD002832.

Vay, S. A., B. E. Anderson, E. J. Jensen, G. W. Sachse, J. Ovarlez, G. L. Gregory, S. R. Nolf, J. R. Podolske, T. A. Slate, and C. E. Sorenson (2000), Tropospheric water vapor measurements over the North Atlantic during the Subsonic Assessment Ozone and Nitrogen Oxide Experiment (SONEX), *J. Geophys. Res.*, *105*, 3745–3755.

Webster, C. R., R. D. May, C. A. Trimble, R. G. Chave, and J. Kendall (1994), Aircraft laser infrared absorption spectrometer (ALIAS) for in situ atmospheric measurements of HCl, N_2O, CH_4, NO_2, and HNO_3, *Appl. Opt.*, *33*, 454–472.

Weinstock, E. M., E. J. Hintsa, A. E. Dessler, J. F. Oliver, N. L. Hazen, J. N. Desmusz, N. T. Allen, L. B. Lapson, and J. G. Anderson (1994), New fast response photofragment fluorescence hygrometer for use on the NASA ER-2 and the Perseus remotely piloted aircraft, *Rev. Sci. Instrum.*, *65*, 3544–3554.

World Meteorological Organization (1957), Meteorology—A three-dimensional science, *WMO Bull.*, *6*, 134–138.

World Meteorological Organization (2003), Scientific assessment of ozone depletion: 2002, *Rep. 47*, Global Ozone Res. and Monit. Project, Geneva.

Zahn, A., and C. A. M. Brenninkmeijer (2003), New directions: A chemical tropopause defined, *Atmos. Environ.*, *37*(3), 439–440, doi:10.1016/S1352-2310(02)00901-9.

Zahn, A., et al. (2000), Identification of extratopical two-way troposphere-stratosphere mixing based on CARIBIC measurements of O_3, CO, and ultrafine particles, *J. Geophys. Res.*, *105*, 1527–1535.

Zöger, M., C. Schiller, and N. Eicke (1999), Fast in situ hygrometers: A new family of balloonborne and airborne Lyman-α photofragment fluorescence hygrometers, *J. Geophys. Res.*, *104*, 1807–1816.

Zondlo, M. A., M. E. Paige, S. M. Massick, and J. A. Silver (2010), Vertical cavity laser hygrometer for the National Science Foundation Gulfstream-V aircraft, *J. Geophys. Res.*, doi:10.1029/2010JD014445, in press.

E. Atlas, Department of Marine and Atmospheric Chemistry, RSMAS, University of Miami, 4600 Rickenbacker Causeway, Miami, FL 33149, USA.

M. A. Avery, G. S. Diskin, M. Loewenstein, J. Lopez, J. R. Podolske, and G. W. Sachse, NASA Ames Research Center, MS 183-401, Moffett Field, CA 94035-1000, USA.

T. Campos, L. L. Pan, S. Tilmes, J. V. Pittman, and A. Weinheimer, Atmospheric Chemistry Division, National Center of Atmospheric Research, PO Box 3000, Boulder, CO 80307-3000, USA. (tilmes@ucar.edu)

L. E. Christensen, R. L. Herman, and C. Webster, Jet Propulsion Laboratory, MS 183-401, 4800 Oak Grove Dr., Pasadena, CA 91109, USA.

R.-S. Gao, Earth System Research Laboratory, NOAA, 325 Broadway, R/CSD 6, Boulder, CO 80305, USA.

E. J. Hintsa, Global Monitoring Division, NOAA, Boulder, CO 80307, USA.

P. Hoor, Institute for Atmospheric Physics, University Mainz, D-55099 Mainz, Germany.

M. E. Paige, Southwest Sciences, Inc., 1570 Pacheco St., Ste. E-11, Santa Fe, NM 87505, USA.

M. R. Proffitt, Proffitt Instruments, 1109 Havre Lafitte Dr., Austin, TX 78746, USA.

C. Schiller and N. Spelten, ICG-1, Research Center Jülich, D-52425 Jülich, Germany.

H. Schlager, Institute for Physics of the Atmosphere, Oberpfaffenhofen, D-82234 Wessling, Germany.

J. Smith, Department of Chemistry and Chemical Biology, Harvard University, Cambridge, MA 02138, USA.

M. A. Zondlo, Center for Mid-Infrared Technologies for Health and the Environment, Department of Civil and Environmental Engineering, Princeton University, Engineering Quad, C-330, Princeton, NJ 08544, USA.